Available online at www.sciencedirect.com

SciVerse ScienceDirect

journal homepage: www.elsevier.com/locate/he

Guidelines for thermal management design of hydride containers

M. Melnichuk [a,b,*], N. Silin [a,c]

[a] CONICET – Concejo Nacional de Investigaciones Científicas y Técnicas, Av. E. Bustillo 9500, CP 8400, S.C. de Bariloche, Río Negro, Argentina

[b] C.N.E.A. – Comisión Nacional de Energía Atómica, Argentina

[c] Instituto Balseiro, Centro Atómico Bariloche (C.N.E.A.), Universidad Nacional de Cuyo, Av. E. Bustillo 9500, CP 8400, S.C. de Bariloche, Río Negro, Argentina

ARTICLE INFO

Article history:
Received 9 April 2012
Received in revised form
23 August 2012
Accepted 9 September 2012
Available online 10 October 2012

Keywords:
Hydrogen storage
Hydride container
Heat transfer
Design

ABSTRACT

Hydrogen storage by means of hydride forming alloys has been intensely studied during last three decades. Container heat management is among the most relevant aspects of study in this field, particularly because in many cases it is the limiting factor for charge and discharge rate. However, given the complexity of the container system and the great variety of possible configurations (type of absorbing material, geometry of the container, hydrogen charge pressure, cooling temperature, etc.), according to the authors' best knowledge, yet there is no general rule for hydride containers design. In this paper we propose general design guidelines using non-dimensional parameters to assess the thermodynamic and kinetics behavior in order to predict the absorption fill up time.

Copyright © 2012, Hydrogen Energy Publications, LLC. Published by Elsevier Ltd. All rights reserved.

1. Introduction

Considering the increase of global pollution and the limited reserves of fossil fuels, there will be a real need to increase the shear of renewable energies in the global energy matrix and to reduce the overall energy consumption. In this context, the importance of hydrogen as a clean energy carrier is that it harmonises the discontinuous generation of renewable energies with continuous electricity demand ("Hydrogen exergizes energy" [1]). The prospective of massive use of hydrogen as an energy carrier implies the need to develop technologies that allow its safe and proper handling.

Hydrogen storage by means of absorbing materials has certain attractive advantages over compressed and liquefied hydrogen: wide range of operating temperatures and pressures including atmospheric conditions, relative safety, reversibility, constant sorption pressure, and high volumetric density. Moreover, the compression work needed when using absorbing materials could be much less than the energy needed to compress or liquefy hydrogen [2].

Hydride containers are very complex systems. Temperature, hydrogen concentration and equilibrium pressure profiles influence kinetics and thermodynamics in a non-linear way along the direction parallel to the heat flow. The release of reaction enthalpy leads to gradients of temperature, which are large given the low thermal conductivity of hydride beds. This results in gradients of reaction rate and an overall increase of the reaction time. Thus, in most situations it is not

* *Corresponding author*. CONICET – Concejo Nacional de Investigaciones Científicas y Técnicas, Av. E. Bustillo 9500, CP 8400, S.C. de Bariloche, Río Negro, Argentina. Tel.: +54 294 4445276; fax: +54 294 4445299.
E-mail address: mmelnichuk@cab.cnea.gov.ar (M. Melnichuk).

0360-3199/$ – see front matter Copyright © 2012, Hydrogen Energy Publications, LLC. Published by Elsevier Ltd. All rights reserved.
http://dx.doi.org/10.1016/j.ijhydene.2012.09.046

Nomenclature

A	area, m^2
α	thermal diffusivity, $m^2\ s^{-1}$
$CHTN$	convective heat transfer number, –
C.S.	control surface
C.V.	control volume
c_p	heat capacity, $J\ kg^{-1}\ K^{-1}$
C_{sg}	hydride capacity, kg H_2/kg hydride, –
$\widehat{C}$	volumetric hydrogen storage capacity, $kg_{H_2}\ m^{-3}$
d	average hydride particle size, m
ΔH	mass enthalpy of reaction, $J\ kg^{-1}$
ΔH^n	molar enthalpy of reaction, $J\ mol^{-1}$
ΔS^n	molar entropy of reaction, $J\ mol^{-1}\ K^{-1}$
e	total energy of control surface/volume, $J\ kg^{-1}$
E_{Abs}	activation energy, $J\ mol^{-1}$
E_{rea}	enthalpy of reaction per unit volume, $J\ m^{-3}$
ε	hydride porosity, –
f_{FC}	constant proportional to fill criteria, –
F	heat conductive material fraction, –
Φ	volumetric flow, $m^3\ s^{-1}$
g	gravity constant, 9.8 $m\ s^{-2}$
k	thermal conductivity, $W\ m^{-1}\ K^{-1}$
κ	kinetics constant, s^{-1}
L	characteristic length, m
MW	molecular weight, $kg\ mol^{-1}$
μ	dynamic viscosity, Pa s
N_{pore}	pore density, m^{-2}
NDC	non-dimensional conductance, –
$NDCW$	non-dimensional compression work, –
$NDFT$	non-dimensional fill time, –
NDK	non-dimensional kinetics, –
$NDHC$	non-dimensional heat capacity, –
$\breve{n}$	normal versor of the control surface, –
P	pressure, bar
$\dot{Q}$	heat power, W
R	ideal gas constant, 8.315 $J\ mol^{-1}\ K^{-1}$
ρ	density, $kg\ m^{-3}$
s	reaction front advance, m
S_m	hydrogen volumetric rate, $kg\ m^{-3}\ s^{-1}$
t	time, s
T	temperature, K
θ	non-dimensional initial temperature, –
u	internal energy, $J\ kg^{-1}$
$\vec{v}$	velocity, $m\ s^{-1}$
V	volume, m^3
VDN	viscous dissipation number, –
$\dot{W}$	work power, W
x	axis "x"
X	hydrogen concentration (fraction of hydrogen capacity), –
z	height, m

Subindex

90%	90% of total capacity
Abs	absorption
cont	container size
d	heat conductive material
des	desired (reaction time)
e	equilibrium
eff	effective
ext	external
g	hydrogen gas
ini	initial
kin	kinetics
max	maximum
pore	pore size
rea	reaction
ref	reference
s	hydride or solid
sys	sensible heat of the container
t	function of time
visc	viscous

possible to assume uniform conditions within the container. That is probably the reason why there is a lack of generalized parameters for hydride containers. Yet there are many experimental and numerical studies of particular cases, i.e.: a defined hydride, inside a container with defined geometry, under defined operational parameters such as hydrogen pressure, external wall temperature, hydrogen flow rate, reaction time, etc.

A non-exhaustive reference list of articles about hydride containers is shown in Table 1. It is organized by groups of hydrides and by the method used to study the hydride container (experimental, numerical or both). This data suggests a prevalence of studies that include both experimental and numerical results, whether or not the experimental results were obtained by the authors or from previous studies. In general, these articles show good correlation between experimental and numerical results. From the table it is also clear that containers filled with AB_5 alloys ($LaNi_5$ and its derivates) are probably the most studied. Moreover, the articles of Table 1 were written during the last decade, indicating that the topic of hydride containers is of present interest.

There are some similarities in the numerical models of the articles of Table 1 that we want to emphasize: many of the studies use a kinetics model based on the one introduced by Mayer et al. [48]. In addition, the thermodynamic models used in most of the papers consider equilibrium pressure as a function of temperature without considering the dependence with hydrogen concentration, while others add an empirical term to account for this dependence [21]. It can be

Table 1 – Articles about hydride containers 2000–2011.

Hydride type	Numerical study	Experimental study	Num. and exp. study
AB_5	[3,4,6,8,9], [5]*, [7]*	[10–12,14,15], [13]*	[16–28,30,32], [29]*, [31]*
Mg	[33]	[34–36]	[37]
Alanate		[38]	[39], [40]*
AB_2	[41,42]	[43–45]	[46]*, [47]

*Propose some sort of optimization.

seen that the way to model the physics of hydride containers is usually the same, thus it should be possible to define a general model for sorption reaction in hydride containers.

An example of a general rule worth mentioning is the one defined by Chaise et al. for the hydraulic losses in hydride containers [49]. They assessed a non-dimensional number called "N" for the hydraulic losses of hydrogen moving though a hydride bed, and after a sensitivity analysis they defined a limit value of N to know if the effect of pressure gradients could be disregarded. This non-dimensional parameter was defined as a function of kinetics, thermodynamic and porosity.

Visaria et al. [50] have developed an interesting non-dimensional conductance (*NDC*) parameter for an AB_2 alloy, which approaches a general rule, but still shows dependence on the thermal condition of the coolant used in their study. They also fixed the desired fill time to 5 min, according to U.S. DoE's targets for mobile applications [51].

In the present work we extend these ideas by adding a non-dimensional fill time parameter (*NDFT*) and evaluating the influence of kinetics and sensible heat. We extend the concept of *NDC* in a simplified system for three hydride forming materials: $Ti_{1.1}CrMn$, $LaNi_5$ and Mg. The selected materials cover a wide range of operational temperatures and pressures. We validated our numerical results with a simple analytical model and with results from previous studies.

2. Numerical model

The purpose of the numerical model is to solve the heat transfer problem together with the hydride formation reaction. The evolution of the latter is dominated by the local thermodynamic conditions, including the temperature, and the reaction kinetics. The numerical solution has two parts for each time step: the determination of the chemical reaction rate and the solution of heat transfer problem to get the evolution of the temperature field.

In the present study we consider the container to be a one-dimensional slab with a fixed external wall temperature and an adiabatic inner thermal condition. For the slab we use a porous medium model. The porous medium assumption requires that the behavior and properties of the studied domain can be averaged in space and time, taking this average for volumes and periods larger than the "texture" of the porous medium ($\sim 10^{-6}$ m) but smaller than the overall size of the domain of interest ($\sim 10^{-2}$ m). A discussion about this topic can be found in the work of Larson and Higdon [52].

We focus on the absorption reaction problem at constant pressure. Several assumptions are made in order to simplify the numerical model but also to simplify the interpretation of the results. Firstly, we assume that the porous medium is homogeneous in the prevalent heat flow direction. Also porosity is constant and independent of hydrogen concentration, and the local thermal equilibrium is valid for the porous medium. We also consider the viscous dissipation, convection and radiating heat transfer to be negligible and we disregard the contact resistance between hydride and container wall. Finally, we assume that specific heat capacities, heat of reaction and thermal conductivity are constant with respect to temperature and hydrogen concentration. These assumptions might be realistic depending on the hydrogen container design and will have to be carefully considered during the assessment of a particular hydrogen container. A more detailed discussion is shown in Appendix A, together with quantitative acceptance criteria for most of the assumptions.

To achieve the solution of the heat transfer problem the numerical model solves the energy equation that involves the phase change enthalpy term. After a detailed analysis of the energy equation shown in Appendix B, we obtained the following simple expression of the heat equation:

$$(\rho c_p)_{eff}\frac{dT}{dt} = \frac{\varepsilon(1-F)}{\rho}\frac{dp}{dt} + S_m\Delta H + \frac{(k_{eff}A\nabla T)_x - (k_{eff}A\nabla T)_{x+dx}}{dV}, \quad (1)$$

where:

$$k_{eff} = (1-F)(\varepsilon k_g + (1-\varepsilon)k_s) + Fk_d, \quad (2)$$

the effective heat capacity $(\rho c_p)_{eff}$ of the mixture is:

$$(\rho c_p)_{eff} = (1-F)\left(\varepsilon\rho_g c_{pg} + (1-\varepsilon)\rho_s c_{ps}\right) + F\rho_d c_{pd}, \quad (3)$$

and the time rate of reacting mass of hydrogen per unit volume of the mixture is:

$$S_m = (1-F)(1-\varepsilon)C_{sg}\rho_s\frac{dX}{dt}, \quad (4)$$

where X is the hydrogen concentration expressed as fraction of hydride capacity and C_{sg} is the total capacity as mass fraction of hydrogen in the alloy.

Thermodynamics is modeled with the equation of Van't Hoff without considering the influence of hydrogen concentration.

$$P_e = P_{ref}\cdot e^{\left(\frac{\Delta H^n_{Abs}}{R\cdot T} - \frac{\Delta S^n}{R}\right)} \quad (5)$$

We employ the kinetics model introduced by Mayer et al. [47], which depends on pressure, temperature and concentration of hydrogen:

$$\frac{dX}{dt} = k_{Abs}\cdot e^{\left(-\frac{E_{Abs}}{R\cdot T}\right)}\cdot\ln\left(\frac{P_g}{P_e}\right)\cdot(1-X) \quad (6)$$

The heat transfer problem is solved by the finite difference method, the details of the implementation are presented in a previous work [30]. The time evolution calculations are performed by an explicit Runge-Kutta algorithm to reduce extrapolation error.

Table 2 shows the parameters used during the simulations for each hydride system, which cover a wide range of temperature and pressure, from room temperature to $T > 300$ °C, and from a relative low pressure (30 bar) to mid pressure (300 bar).

3. Results and discussion

3.1. Heat transfer analysis

We used the non-dimensional conductance defined by Visaria et al. as starting point [50]. This parameter is defined as the

Table 2 – Parameters of the simulations.

Parameter	$Ti_{1.1}CrMn$	$LaNi_5$	Mg
c_{ps} (J kg^{-1} K^{-1})	500	355	120
ΔH^n_{Abs} (J mol^{-1})	−14,390	−30,478	−75,000
ΔS_{Abs} (J mol^{-1} K^{-1})	−91.3	−108	−133.5
E_{Abs} (J mol^{-1})	20,700	21,170	1.24×10^5
κ_{Abs} (s^{-1})	150	59.2	2.90×10^8
C_{sg}	0.015	0.0128	0.06
k_s (W m^{-1} K^{-1})	1	1	0.5
ε	0.6	0.5	0.7
ρ_s (kg m^{-3})	2500	8310	1740
Reference	[50]	[52]	[37]
T_{ext} (°C)	20	20	327
P_g (bar)	300	30	30

rate of the heat dissipation that can be evacuated by conduction $\dot{Q}_{dis}$, to the heat generation rate $\dot{Q}_{rea}$ for the reaction to take place in a desired reaction time t_{des}.

$$NDC = \frac{\dot{Q}_{dis}}{\dot{Q}_{rea}} \tag{7}$$

$$\dot{Q}_{dis} = \frac{(T_{\max} - T_{ext})}{L/k_{eff}} \tag{8}$$

$$\dot{Q}_{rea} = E_{rea} \cdot \frac{L}{t_{des}} \tag{9}$$

$$E_{rea} = \Delta H_{abs} \cdot C_{sg} \cdot \rho_s \cdot (1-\varepsilon) \cdot (1-F), \tag{10}$$

where E_{rea} is the enthalpy of reaction per unit volume.

Therefore the parameter *NDC* is a measure of the fraction of heat generation rate due to hydriding that can be removed by a hydride container. Higher values of NDC correspond to higher heat transfer rates.

The term $\dot{Q}_{dis}$ considers a temperature difference divided by a thermal resistance. For the sake of simplicity we only consider the effective thermal conductivity of the porous material, neglecting contact thermal resistances, radiation heat transfer and convective effects. Temperature $T_{\max}$ is a function of the absorption pressure and is fixed by the Van't Hoff equation. The term $\dot{Q}_{rea}$ considers heat of reaction, capacity and porosity of the hydride, and it should also consider heat conductive material if present, through the term *F*. The thickness of the hydride appears as L^2 in Eq. (7) when reordered, so it has a relative high weight in this parameter.

We think that the parameter *NDC* is a very useful design tool for hydride containers since it relates:

- *Hydride properties*: $\Delta H_{Abs} C_{sg} \rho_s (1-\varepsilon)$. The convenience of the selected hydride is assessed by these properties, which usually can barely be modified.
- *Operational conditions*: $(T_{\max} - T_{ext})t_{des}$. These parameters include hydrogen charge pressure (indirectly expressed with $T_{\max}$), temperature of the heat exchange surface (which will be proportional to the temperature and the means used to dissipate heat from the container), and the time intended for the absorption reaction to occur up to a defined fill criteria.
- *Design parameters*: $k_{eff}/L^2(1-F)$. In this case k_{eff} may be increased by introducing a high thermal conductivity material, such as aluminum. Therefore, both k_{eff} and *F* are proportional to the amount of conductive material. L^2 represents the effective length of the heat path within the hydride towards the wall of the heat exchange system. Examples of this characteristic length are: the half thickness of hydride between fins, the half size of the average pore of a metal foam, the radius of a hydride container without heat transfer system, etc. These parameters are usually limited by technology and cost.

We define a non-dimensional fill time by dividing the time needed to reach 90% of the maximum hydrogen concentration in the hydride bed ($t_{90\%}$) by the desired reaction time (t_{des}) used in the *NDC* parameter.

$$NDFT = \frac{t_{90\%}}{t_{des}} \tag{11}$$

With these elements, we analyze the relation between *NDC* and *NDFT* for the hydrides $Ti_{1.1}CrMn$, $LaNi_5$ and Mg (Fig. 1). In order to simplify the analysis we multiply the kinetics constant by a factor 10^2 and we divided the heat capacity by a factor 10. After sensitivity analysis, we confirmed the stability of this simplified approach, which provides results independent from the sorption kinetics and the heat capacity of the hydride.

In Fig. 1 we analyze the effect of an increase of $\dot{Q}_{dis}$ (Eq. (8)) and thus of *NDC*. This can be done in different ways: by increasing hydrogen charge pressure P_g and thus increasing $T_{\max}$, by reducing the temperature of the cold source T_{ext}, by increasing the effective thermal conductivity k_{eff} using a high conductivity material, or by reducing hydride thickness *L*. According to Fig. 1 the reaction time decreases with *NDC*. For $NDC >> 1$ this effect is not significant, but probably a waste of resources.

Under the mentioned conditions, the three hydride systems show the same behavior so that the results of the three hydrides can be fitted with the following equation:

$$NDFT = f_{FC} NDC^{-1}, \tag{12}$$

where $f_{FC} = 0.43$.

This result means that in order to obtain a reaction time $t_{90\%}$ equal or lesser than the desired time ($NDFT \leq 1$), according to our numerical results, $\dot{Q}_{dis}$ should be at least 43% of $\dot{Q}_{rea}$.

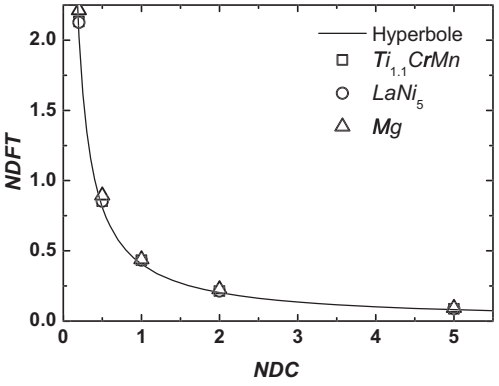

Fig. 1 – NDC vs. NDFT for $Ti_{1.1}CrMn$, $LaNi_5$ and Mg.

The parameter f_{FC} is a function of the defined Fill Criteria, in this case 90%.

Because of the simplifications done to the model of the container system, Eq. (12) can also be obtained by analytical solution of the Stefan problem with no heat capacity term [53]. When heat capacity is negligible and reaction kinetics has no influence in the absorption reaction, the reaction takes place as a reaction front. A scheme of the resulting temperature profile is shown in Fig. 2, where the hydride phase (reacted material) will be just a thermal resistance to the heat flow. Considering the reaction front model, the heat flux needed for the absorption reaction is equal to the energy of reaction per unit volume E_{rea} (Eq. (10)) multiplied by the velocity of the reaction front $\partial s_t/\partial t$. Then, considering the Fourier law of conduction we obtain:

$$\dot{Q} = \frac{\partial s_t}{\partial t} E_{rea} = -k_{eff} \frac{(T_{max} - T_{ext})}{s} \tag{13}$$

Integrating and using the initial boundary condition $s = 0$ for $t = 0$, we obtain a function that correlates the elapsed time of reaction and the position of the reaction front:

$$t = \frac{1}{2} s^2 \frac{E_{rea}}{k(T_{max} - T_{ext})} \tag{14}$$

According to this model, $t_{90\%}$ will be reached when the reaction front has advanced 90% of L. Then,

$$t_{90\%} = \frac{1}{2}(0.9L)^2 \frac{E_{rea}}{k_{eff}(T_{max} - T_{ext})} = f_{FC}\big|_{Analytical} \frac{E_{rea} L^2}{k_{eff}(T_{max} - T_{ext})} \tag{15}$$

For this analytical case $f_{FC}\big|_{Analytical} = 0.405$. This result confirms the one obtained numerically, supporting the hyperbole fitting performed in Fig. 1.

Moreover, Fig. 3 shows temperature and hydrogen concentration profiles for a $Ti_{1.1}CrMn$ container filled up to 50% of the total hydride capacity. The shape of these curves is similar to the shape of the idealized curves of the Stefan problem (Fig. 2).

3.2. Kinetics influence

If we perform a simulation with the actual hydride forming kinetics, we will have a longer filling time respect to the simplified case analyzed in the previous section. This can be seen as obtaining a larger value of f_{FC} ($f_{FC} = NDC \times NDFT$). It is important to be able to estimate the influence of the hydride forming kinetics in the total reaction time. In order to address this influence, we define a non-dimensional kinetics (NDK) number in a similar fashion to the definition of the NDC. In this case the parameter NDK is defined as the average heat generation rate $\dot{Q}_{kin}$ for the reaction limited only by the kinetics characteristic time t_{kin} to the rate of the heat dissipation rate by conduction $\dot{Q}_{dis}$. We obtain the following parameter:

$$NDK = \frac{\dot{Q}_{kin}}{\dot{Q}_{dis}}, \tag{16}$$

where

$$\dot{Q}_{kin} = E_{rea} \frac{L}{t_{kin}} \tag{17}$$

and

$$t_{kin} = \left[k_{Abs} e^{-\frac{E_{Abs}}{R T_{ext}}} \ln\left(\frac{P_g}{P_e}\right) \right]^{-1}. \tag{18}$$

The characteristic time for hydride forming kinetics t_{kin} is calculated from the hydride's constants k_{Abs}, E_{Abs} and the absorption parameters P_g and T_{ext}. Absorption reaction will occur at a temperature between T_{ext} and T_{Max}, yet we considered T_{ext} as a more representative temperature for the calculation of t_{kin} because it is at the lowest temperature that the kinetics play a more relevant role. In other words, the faster reaction rate occurs at T_{ext} and that is the situation where kinetics becomes more relevant.

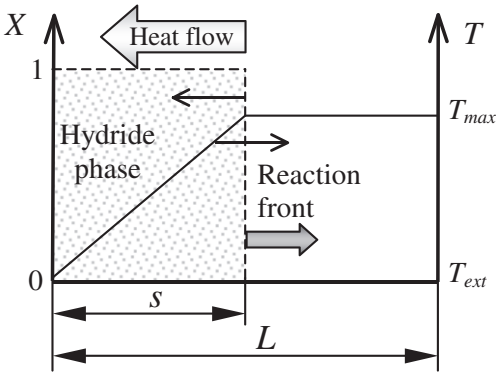

Fig. 2 – Ideal temperature and hydrogen concentration scheme for $0 < t < t_{90\%}$, when heat capacity and kinetics have no influence in the absorption reaction.

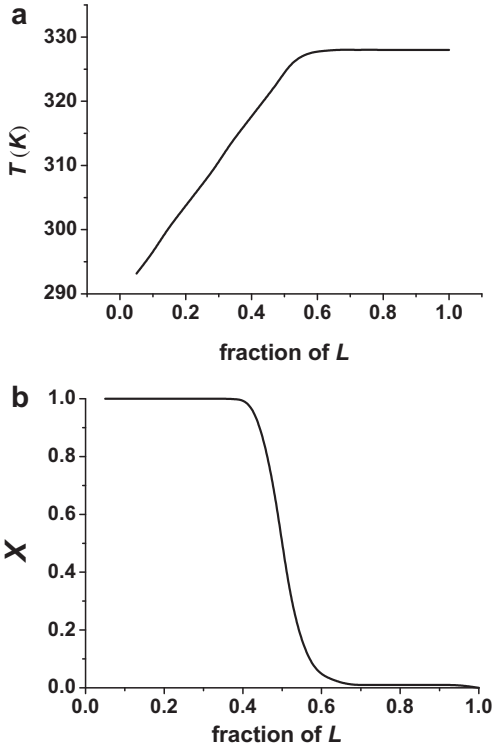

Fig. 3 – (a) Temperature profile and (b) hydrogen concentration profile for 50% reaction $Ti_{1.1}CrMn$.

The parameter *NDK* is useful to determine whether the operational and geometrical conditions are such that kinetics has a relevant influence. Fig. 4 shows *NDK* vs. *NDC* × *NDFT* for *NDC* = 1. Variation of *NDK* was achieved by multiplying k_{Abs} by arbitrary factors, while heat capacity was divided by 10 in order to minimize its influence. The definition of t_{des} is irrelevant in this figure since it is not present in *NDK* and it is cancelled out in *NDC* × *NDFT*.

In Fig. 4 we added a line for $f_{FC} = NDC \times NDFT = 0.405$, i.e. the result for instantaneous kinetics. We can observe that for *NDK* > 1 kinetics influence decreases rapidly, and the value of *NDC* × *NDFT* tends asymptotically to 0.405. From the figure it is also clear that for *NDK* >> 1 the difference between hydrides is not important.

3.3. Heat capacity influence

In order to verify the effect of sensible heat we modify the heat capacity of the hydride container for the different hydrides under study. As before, we define a non-dimensional heat capacity (*NDHC*) parameter to quantify the influence of sensible heat in the reaction time as follows:

$$NDHC = \frac{E_{sys}}{E_{rea}}, \tag{19}$$

where,

$$E_{sys} = (\rho c_p)_{eff}(T_{max} - T_{ini}) \tag{20}$$

The term E_{sys} represents the sensible energy per unit volume of hydride needed to increase its temperature from T_{ini} to T_{max}. Fig. 5 shows the results of *NDC* × *NDFT* as a function of *NDHC*, for *NDC* = 1. Kinetics constants remain unaltered, leading to *NDK* > 1 in the three cases under study. We have taken values of T_{ini} equal to T_{ext}.

Results for $Ti_{1.1}CrMn$ and $LaNi_5$ are somehow intuitive: an increase of heat capacity creates an additional heat absorption in the container, therefore decreasing the total fill time. In the case of Mg the increased heat capacity leads to sustained low temperatures and therefore slower kinetics, leading to an increase in *NDFT* ($dX/dt \propto f(T)$). This effect is only relevant in the Mg system because its kinetics is more dependent on temperature than for $Ti_{1.1}CrMn$ or $LaNi_5$ systems. This fact can be seen by the kinetics parameters of Table 2, which are various orders of magnitude larger in comparison. It should also be noted that according to Askri et al. [54], radiation cannot be disregarded as heat transfer mechanism in Mg hydride containers because of its relative high operational temperature.

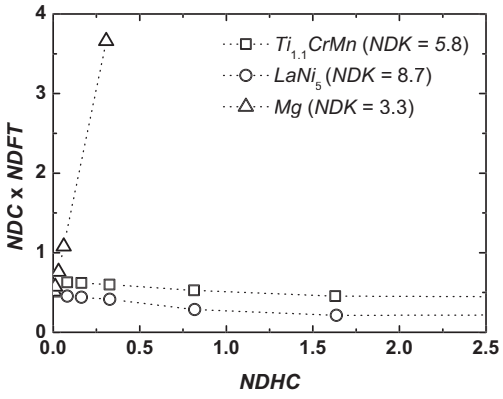

Fig. 5 – *NDHC* vs. *NDC* × *NDFT* for $Ti_{1.1}CrMn$, $LaNi_5$ and Mg.

In spite of the uncertainties mentioned in the last paragraph, we think that as a general rule heat capacity has a minor influence since the values calculated with typical alloy properties are *NDHC* < 0.16 for $Ti_{1.1}CrMn$ and $LaNi_5$, and *NDHC* < 6×10^{-3} for Mg.

3.4. Design parameters of previous experimental results

We calculate the parameters *NDC* vs. *NDFT* using previously reported results in order to verify the non-dimensional parameters design approach introduced in this paper against actual experimental devices. Fig. 6 shows *NDC* vs. *NDFT* results assuming t_{des} = 5 min in order to facilitate the comparison, and following the criteria adopted by Visaria et al. [50]. The experimental results from different authors show good correlation with the general hyperbole defined by Eq. (12), even though these results have real kinetics and sensible heat parameters. The fact that some results appear below or too separated from the hyperbole is attributed to the simplifications assumed for the parameters adopted in each case, particularly the assumption of a unique thermal

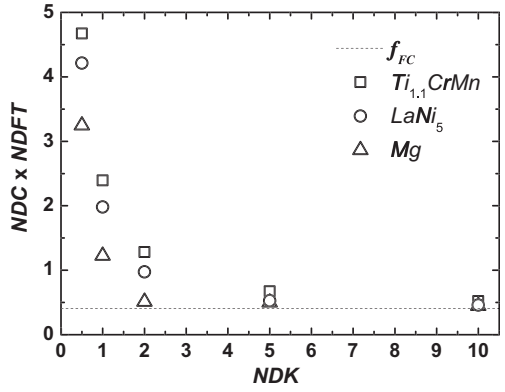

Fig. 4 – *NDK* vs. *NDC* × *NDFT* for $Ti_{1.1}CrMn$, $LaNi_5$ and Mg.

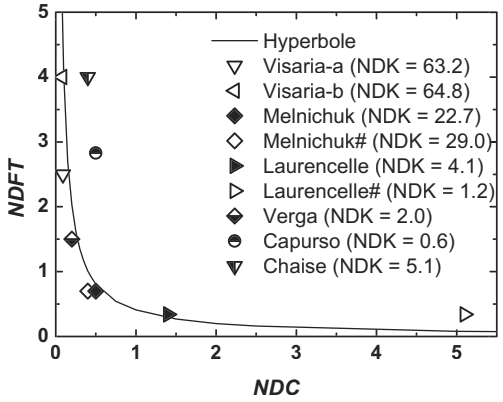

Fig. 6 – *NDC* vs. *NDFT* from references for t_{des} = 5 min.

conductivity and the characteristic length, that in many cases should be representative of complex geometries in two or three dimensions. A short description of the assumptions made for each case is presented in Appendix C.

Results assessing the importance of kinetics are depicted in Fig. 7 (*NDK* vs. *NDC* × *NDFT*). These results are in agreement with the numerical results of Fig. 4. The fact that results obtainer from Capurso, Chaise and Laurencelle# show higher *NDC* × *NDFT* values is consistent with their low *NDK*, and it can be related to the distance of the respective points to the hyperbole of Fig. 6, suggesting that these experimental systems were dominated by kinetics restrictions rather than heat transfer.

Additionally for systems involving heat management elements such as small fins, i.e. the work of Melnichuk et al. [30] or foams, i.e. the work of Laurencelle et al. [55], we performed the analysis at two different scales. One is the "pore", or microscopic scale (denominated Laurencelle# and Melnichuk#), for the volume of hydride bounded by the conductive material (foam or fin), and the other is the whole container or macroscopic scale (denominated Laurencelle and Melnichuk). The experiments of Melnichuk et al. involved a reactor with a large characteristic length and a high fraction of homogeneous extended surface ($F = 0.33$). Results between pore size and container size analysis show little difference. On the other hand, the results of Laurencelle et al. using aluminum foam ($F = 0.09$) show longer reaction times for pore size analysis than results considering the whole container with a homogeneous thermal conductivity. Therefore, for this case we can see that the heat transfer inside the pore is the limiting factor in the container dynamics.

3.5. *Non-dimensional equations*

Finally, using the non-dimensional parameters introduced in previous sections we can express the equations in non-dimensional form. The one-dimensional heat equation (Eq. (1)) can be rewritten as follows:

$$(\rho c_p)_{eff}\frac{\partial T}{\partial t} = \frac{\varepsilon(1-F)}{\rho_g}\frac{\partial P}{\partial t} + S_m \Delta H_{abs} + \frac{\partial\left(k_{eff}\left(\frac{\partial T}{\partial x}\right)\right)}{\partial x} \tag{21}$$

To make this equation non-dimensional we will adopt the following non-dimensional variables:

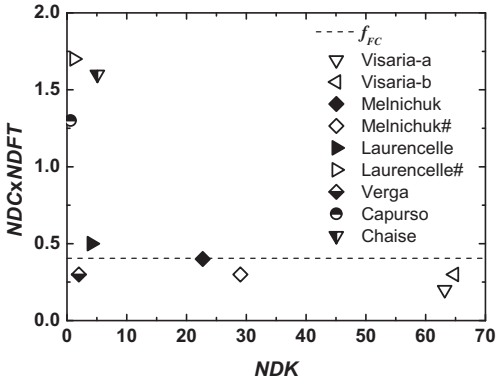

Fig. 7 – *NDK* vs. *NDC* × *NDFT* from previous results.

$$T^* = \frac{T}{T_{max} - T_{ext}} \tag{22}$$

$$t^* = \frac{t}{t_{des}} \tag{23}$$

$$P^* = \frac{P}{P_g - P_{ini}} \tag{24}$$

$$\frac{\partial X}{\partial t^*} = S_m^* = \frac{t_{des}}{C_{sg}\rho_s(1-\varepsilon)(1-F)} S_m \tag{25}$$

where P_{ini} is the pressure inside the container before the charge process begins. It should be noted that Eq. (25) is the non-dimensional form of Eq. (4). Replacing these expressions into Eq. (21) and considering k_{eff} constant we obtain the non-dimensional heat equation:

$$NDHC\ \ \theta_{ini}^{-1}\frac{\partial T^*}{\partial t^*} = NDCW\frac{\partial P^*}{\partial t^*} + \frac{\partial X}{\partial t^*} + NDC\frac{\partial^2 T^*}{\partial t^{*2}} \tag{26}$$

Here,

$$NDCW = \frac{(P_g - P_{ini})\varepsilon(1-F)}{E_{rea}} \tag{28}$$

$$\theta_{ini} = \frac{(T_{max} - T_{ini})}{(T_{max} - T_{ext})} \tag{29}$$

Note that the influence of the heat capacity is related to the initial temperature T_{ini} rather than the external temperature T_{ext} used in the other non-dimensional groups, therefore the non-dimensional initial temperature θ_{ini} appears in the heat capacity term.

We obtain a new non-dimensional parameter related to the compression work that we called *NDCW* and shows the relative importance of the compression work compared to the reaction energy. This parameter has shown to be very small for the cases studied so that the whole term may be neglected.

It is worth noting that the reaction kinetics does not show up in the non-dimensional heat equation (Eq. (26)). To bring up the relation between the reaction kinetics and the thermal evolution in terms of non-dimensional numbers we can analyze the kinetics model expressed by Eq. (6). We can make this equation non-dimensional by the introduction of a kinetic characteristic time t_{kin}:

$$\frac{\partial X}{\partial \tilde{t}} = t_{kin}\frac{\partial X}{\partial t} \tag{30}$$

According to Eq. (6) we adopt a characteristic time t_{kin} calculated at the external temperature T_{ext} and the corresponding equilibrium pressure $P_e(T_{ext})$, then we get:

$$t_{kin} = \left[k_{abs} e^{\left(-\frac{E_{abs}}{RT_{ext}}\right)} \ln\left(\frac{P_g}{P_e(T_{ext})}\right)\right]^{-1} \tag{31}$$

which can be regarded as the inverse of the initial reaction velocity of the hydride forming material at temperature T_{ext} (notice X is non-dimensional). To evaluate the role of reaction kinetics as compared to thermal dynamics in the overall system evolution, we can compare the corresponding characteristic times, t_{kin} and t_{des} respectively. The ratio of these two

characteristic times can then be expressed in terms of the non-dimensional parameters *NDK* and *NDC* as follows:

$$\frac{t_{des}}{t_{kin}} = \frac{E_{rea}L/t_{kin}}{\dot{Q}_{dis}} \frac{\dot{Q}_{dis}}{E_{rea}L/t_{des}} = NDK \times NDC \quad (32)$$

A thermally optimized system should have an $NDC \approx 1$. Then a high value of *NDK* indicates that the kinetics characteristic time is small and therefore not a limiting factor in the system dynamics.

4. Conclusions

In the present work we propose a set of non-dimensional parameters that can be used as a guideline for the design and assessment of the thermal aspects of hydride containers. For this purpose we use a one-dimensional numerical model that simulates heat transfer and reaction kinetics. The numerical model was verified against a simple analytical model for cases where reaction kinetics and heat capacity are negligible. Numerical results were also consistent with results from previously reported measurements.

For the assessment of the thermal behavior of the hydride container, hydride properties, operational conditions and design parameters were combined into a single non-dimensional parameter, i.e. the non-dimensional conductance *NDC* proposed by Visaria et al. [50], being the single most important parameter to consider in most cases. The filling time was assessed trough the non-dimensional fill time *NDFT*, which in the case of heat transfer dominated systems becomes inversely proportional to *NDC*.

The influence of the reaction kinetics was evaluated through a non-dimensional kinetics parameter *NDK*. In the same way the heat capacity of the hydride container (hydride-conductive material mixture) was evaluated through the non-dimensional heat capacity parameter *NDHC*. The value of $NDC \times NDFT$, which is constant for heat conduction dominated systems, increases when $NDK < 1$ as the system becomes dominated by the reaction kinetics. On the other hand the effect of higher heat capacity, i.e. higher *NDHC*, is more difficult to predict and depends on several factors. Yet for real systems the value of *NDHC* is low making it unimportant for most situations.

We think that this set of parameters allows the system designer to evaluate approximately whether the heat management system is suit for his design, and if the reaction kinetics will be relevant in the sorption process.

As future work we think that a more exhaustive study could be useful, extending the present analysis to systems with more complex thermodynamics such as alanates and to different fill criteria.

Acknowledgements

The authors want to thank the following colleagues for their valuable discussions: Dr. Marcos Sade, Dr. Facundo Castro, Dr. Fabiana Gennari, Dr. Gabriel Meyer, Dr. Alberto Baruj, Dr. Horacio Troiani, Lic. Natalia Salva and specially Dr. Hernán Peretti. The financial support of Argentinean scientific institutions CONICET, ANPCyT and CNEA is also acknowledged.

Appendix A. Model assumptions

In this section we discuss the pertinence of the assumptions made on this work. We tried to include non-dimensional parameters when possible to help deciding about the relevance of these assumptions.

A.1. Porous medium is homogeneous

We use a porous medium model which means that the microscopic behavior is averaged in space and time. We are analyzing cases where the porous medium does not vary in the heat transfer direction. For a non-homogeneous system, i.e. as presented in the work of Melnichuk et al. [30], the set of non-dimensional parameters (*NDC*, *NDFT*, *NDK* and *NDHC*) can still be used. If the representative parameters selected of the non-dimensional numbers are correctly defined, the same general tendencies should be expected, but obviously with different threshold values that will depend on the nature of the non-homogeneity.

A.2. Heat transfer is one-dimensional

This assumption is geometrical and implies that from the macroscopic point of view, i.e. the porous medium approach, temperature gradients and energy flows should be prevalent in this direction. This is a good approximation in most cases given that the dimension of the porous medium in the heat flow direction is much shorter than the other dimensions.

A.3. Porosity is constant and independent of hydrogen concentration

This assumption is not strictly valid but is a necessary approximation. For most hydride forming alloys the porosity is modified by the volumetric expansion of the hydride during the sorption process. For example, AB_5 alloys may expand about 20% in volume. Thus this simplification adds an error in the effective thermal conductivity of the hydride and in the expansion volume. When a high conductivity material such as aluminum is introduced to improve the porous medium conductivity, the evolution of the thermal conductivity of the hydride becomes irrelevant, as the heat transfer is dominated by material with high conductivity. On the other hand, the variation of the expansion volume affects the work term in the energy equation (Eq. (1)), which is already a minor contributor to the enthalpy of the system. We discuss the porous medium thermal conductivity further in Section A.7. Finally it should be noted that these effects are not relevant when compared with the uncertainties in the hydride properties available in the literature.

A.4. Local thermal equilibrium is valid for the porous medium

The hypothesis of local thermal equilibrium should be analyzed in each particular case. A detailed analysis of a particular case would probably require 2D or 3D simulations or a proper experimental test. We considered that this hypothesis is generally valid for hydride systems with no

addition of conductivity enhancing materials, particularly considering that the particle size ($\sim 10^{-6}$ m) is normally much smaller than characteristic length ($\sim 10^{-2}$ m). In the case of a hydride system with additional conductive material, such as aluminum foam, fins, honey comb profile, etc., it would be necessary to analyze the microscopic scales, i.e. the pore scale, and to evaluate whether local thermal equilibrium can be assumed. We suggest to do this by performing a microscopic analysis, considering firstly the heat transfer problem from the hydride to the fins or other conductivity enhancing materials. This heat transfer should be significantly more efficient than the overall heat transfer. One way of doing this is to calculate a microscopic *NDC* using microscopic dimensions and considering the hydride as porous medium, this should produce a "microscopic *NDC*" much higher than the "macroscopic *NDC*". This type of microscopic analysis is performed in point 3.4.

A.5. *Viscous dissipation is negligible*

It should be noted that the viscous dissipation is highly variable upon the gas flow paths which may differ highly between different designs, even between those that can be regarded one-dimensional from the heat transfer point of view. We can think of two possible effects due to the viscosity of hydrogen. One is the generation of pressure gradients that would slow down the reaction, i.e. changing the local value of P_g. This was already addressed by Chaise et al. [49]. Another effect is the generation of viscous dissipation heat. We define a non-dimensional parameter called viscous dissipation number (*VDN*):

$$VDN = \frac{\dot{Q}_{visc}}{\dot{Q}_{rea}} \tag{A1}$$

where $\dot{Q}_{visc}$ is the heat power due to viscous dissipation and $\dot{Q}_{rea}$ is defined in Eq. (9).

Because of the small scales and velocities involved the flow through the porous medium composed by the metal hydride it is expected to be laminar. To obtain an approximate value of the pressure we analyze a pore of circular cross-section. For a small volume including one of these pores we define $\dot{Q}_{visc}$ as function of the hydride length as follows:

$$\dot{Q}_{visc} = \int_0^L \frac{dP}{dx} \cdot \frac{\Phi(x)}{A} dx \tag{A2}$$

where dP/dx is the local pressure loss per unit length and Φ is the volumetric flow of hydrogen gas across the area *A* normal to the flow direction.

Given that the flow through the porous medium is slow and the characteristic pore size is extremely small we can use a Darcy model for the flow resistance, though that requires a knowledge of the friction law for the specific porous medium that is being analyzed. Here to estimate dP/dx, we approximate the pores as cylindrical tubes and use the Hagen–Poiseuille equation:

$$\frac{dP}{dx} = \frac{128 \mu \Phi_{pore}(x)}{\pi d^4} \tag{A3}$$

where μ is the dynamic viscosity of the hydrogen and *d* the diameter of passage of hydrogen.

If we consider that the volumetric flow rate is constant, we can consider that the reaction kinetics is constant. Then:

$$\frac{dX}{dt} \approx \frac{0.9}{t_{90\%}} \tag{A4}$$

The volumetric flow rate is defined in the *x* direction as follows:

$$\Phi(x) = A \int_0^x \frac{1}{\rho_g} \left(\widehat{C} \frac{dX}{dt} \right) dx = A \frac{\widehat{C}}{\rho_g} \frac{0.9}{t_{90\%}} x \tag{A5}$$

$$\widehat{C} = C_{sg} \rho_s (1-\varepsilon)(1-F) \tag{A6}$$

$$\Phi_{pore}(x) = \frac{\Phi(x)}{A} \times (N_{pore})^{-1} \tag{A7}$$

where, if we assume pores with circular cross-section, the pore density can be calculated as: $N_{pore} = 4\varepsilon/\pi d^2$. Using Eqs. (A2), (A3) and (A7) we finally get:

$$\dot{Q}_{visc} = \frac{32 \mu}{3\varepsilon} L^3 \left(\frac{\widehat{C}}{\rho_g d} \frac{0.9}{t_{90\%}} \right)^2 \tag{A8}$$

Now we can evaluate the non-dimensional fraction of viscous dissipation:

$$VDN = \frac{\dot{Q}_{visc}}{\dot{Q}_{rea}} = \frac{\frac{32 \mu}{3\varepsilon} L^3 \left(\frac{\widehat{C}}{\rho_g d} \frac{0.9}{t_{90\%}} \right)^2}{\Delta H_{abs} \cdot \widehat{C} \frac{L}{t_{des}}} = \frac{32 \cdot (0.9)^2 \mu \widehat{C} L^2 t_{des}}{3\varepsilon d^2 \rho_g^2 \Delta H_{abs} t_{90\%}^2} \tag{A9}$$

To estimate the order of magnitude of Eq. (A9) we consider typical parameters for H_2 and $LaNi_5$ assuming $t_{des} \sim t_{90\%}$ for a thermally optimized system:

$\mu_g \approx 9 \times 10^{-6}$ Pa s
$C_{sg} = 0.01$
$\rho_s = 8300a\ kg_{HM}\ m^{-3}$
$(1-\varepsilon) = 0.5$
$(1-F) = 0.9$
$\rho_g\big|_{P=20\ bar,\ T=27\ ^\circ C}\ 8.9 \times 10 = 1.6\ kg_{H_2}\ m^{-3}$ [59]
$L \approx 3 \times 10^{-2}$ m
$d \approx 3 \times 10^{-6}$m
$t_{90\%} = 300$ s
$\Delta H_{abs}^n = 3 \times 10^5\ J\ mol_{H_2}$
$MW_{H_2} = 2 \times 10^{-3}\ kg_{H_2}\ m^{-3}$
$\Delta H_{abs} = \Delta H_{abs}^n \times MW_{H_2}^{-1}$
$\rightarrow VDN = 5.6 \times 10^{-6} \rightarrow$ negligible

Therefore the heat power due to viscous dissipation is negligible when compared to heat of reaction.

A.6. *Convection heat transfer is negligible*

In this work we defined a physical model where gas flow is perpendicular to the heat flow (see Figure B1), thus convection is irrelevant. However, configurations with parallel gas and heat flow are possible. Then we analyze this type of container

configuration by defining a non-dimensional parameter called convective heat transfer number (*CHTN*) as follows,

$$CHTN = \frac{\dot{Q}_{conv}}{\dot{Q}_{cond}} \tag{A10}$$

where $\dot{Q}_{conv}$ is the convection heat transfer and $\dot{Q}_{cond}$ is the conduction heat transfer. These terms can be calculated by means of the convection–diffusion equation, whose general form is:

$$\frac{\partial c}{\partial t} = \nabla(D\nabla c) - \nabla\left(\vec{v}c\right) \tag{A11}$$

where c is the variable of interest, in our case $c = \rho_g c_{pg} T$, and D is the diffusivity, in our case $D = \alpha = k_{eff}/\rho_g c_{pg}$.

Now we analyze the conduction term, i.e. the first term on the right hand side of Eq. (A11):

$$\dot{Q}_{cond} = \nabla(D\nabla c) \overset{1D}{\rightarrow} \frac{\partial}{\partial x}\left(\frac{k_{eff}}{\rho_g c_{pg}}\frac{\partial\left(\rho_g c_{pg} T\right)}{\partial x}\right) \tag{A12}$$

Considering that density and specific heat of gas are independent from x, and approximating $\partial^2 T/\partial x^2 \propto (T_{max} - T_{ext})/L^2$, we obtain:

$$\dot{Q}_{cond} = \frac{k_{eff}(T_{max} - T_{ext})}{L^2} \tag{A13}$$

The convection term is also obtained from Eq. (A11):

$$\dot{Q}_{conv} = \nabla\left(\vec{v}c\right) \overset{1D}{\rightarrow} \rho_g c_{pg}\frac{\partial\left(\vec{v}T\right)}{\partial x} \tag{A14}$$

This term is variable in x and will change in time. However we can obtain an order of magnitude estimation using Eq. (A5) to estimate the velocity and using $(T_{max} - T_{ext})/L$ to approximate the temperature gradient:

$$\dot{Q}_{conv} \propto \rho_g c_{pg}\left(\frac{\Phi}{A}\right)\frac{(T_{max} - T_{ext})}{L} \approx c_{pg}\frac{\widehat{C}}{t_{90\%}}(T_{max} - T_{ext}) \tag{A15}$$

With Eqs. (A13) and (A15), Eq. (A10) becomes:

$$CHTN = \frac{c_{pg}\widehat{C}L^2}{t_{90\%}k_{eff}} \tag{A20}$$

We estimate the order of magnitude of Eq. (A20) using the typical parameters for H_2 and $LaNi_5$ used for Eq. (A13), plus the following parameters:

$c_{pH_2} = 14{,}266\ J.kg^{-1}.K^{-1}$
$k_{eff} = 1\ W.m^{-1}.K^{-1}$
$\rightarrow CHTN = 1.6.$

That is to say that for a container configuration where gas and heat flows are parallel, the convection heat transfer is not negligible. If the configuration is such that the gas flows against the temperature gradient it will help the heat transfer and otherwise it might be detrimental.

A.7. Radiative heat transfer is negligible

Assuming that contact resistance is negligible, radiation heat transfer between hydride bed and the container wall is irrelevant (see Section A.8). A different case is the radiation between hydride particles, which changes the effective thermal conductivity of the powder. In Section 3.3 we have observed that the radiation heat transfer mechanism could have an effect of MgH_2 systems due to their high temperature and to the fact that radiation heat transfer depends on temperature with a power of four [54]. The analysis of radiation heat transfer involves the particles transmittance, reflectivity and view factors, and involves particles with sizes in the order of magnitude of the radiation wavelengths. All this makes the modeling of radiation heat transfer a rather complex issue that exceeds the scope of this paper.

A.8. The contact resistance between the porous medium and the container walls is negligible

For the sake of simplicity we have assumed the contact resistance is much smaller than the thermal resistance of the porous medium of thickness L. Yet if there were a gap between the porous medium and the walls the contact resistance can become prevalent. The contact resistance varies depending on the container design and during the hydride forming process due to swelling, it is therefore a relevant design aspect. In the case of the article of Visaria, where *NDC* parameter was first defined [50], they considered thermal conductivity (L/k_{eff}), convection heat transfer (h_f) and contact resistance (R_{tc}). In their study they analyzed different values of contact resistance, including $R_{tc} = 0$. There is no simple model for the contact resistance and a detailed analysis exceeds the scope of this work.

A.9. The specific heat capacity, heat of reaction and thermal conductivity are assumed to be constant with respect to temperature and hydrogen concentration

These three thermal properties have been taken as constant. The specific heat capacity is very difficult to measure, particularly near the phase change conditions, and therefore it has a large associated error. On the other hand, the heat capacity plays a minor role and therefore the heat capacity may well be taken as constant.

The heat of reaction on the other hand is a relevant parameter but it is constant well within the relative errors of other parameters.

A completely different situation happens with the thermal conductivity of the hydride forming alloy. The effective thermal conductivity of the hydride is strongly influenced by pressure, hydrogen concentration and temperature, varying as much as an order of magnitude. However, if effective thermal conductivity is significantly improved by the addition of a high conductivity material, hydride thermal conductivity becomes irrelevant and the overall effective conductivity can be considered to be constant.

Appendix B. One-dimensional heat equation

In this section we propose a one-dimensional model for the thermal problem and present the developments of the equations in detail as we consider this is missing from available

bibliography. We also hope this will help other researchers to clarify the energy balances involved.

To obtain the one-dimensional heat equation for this problem we start with the total energy conservation equation [56]:

$$\dot{Q} - \dot{W} = \frac{d}{dt}\int_{C.S.} \rho e \, dV + \int_{C.S.} \rho e\left(\vec{v}\cdot\breve{n}\right) dA \tag{B1}$$

with:

$$e = u + \frac{1}{2}\vec{v}^2 + gz \tag{B2}$$

In the present case neither kinetics energy nor potential energy are relevant and heat capacity can be considered constant, so we can take

$$e = u = c_p T - P/\rho \tag{B3}$$

We shall consider fixed control volumes where only pressure mechanical work can occur, thus:

$$\dot{W} = \int_{C.S.} \frac{P}{\rho}\rho\left(\vec{v}\cdot\breve{n}\right) dA \tag{B4}$$

We will also consider conduction ($-k\nabla T$) as the only heat input mechanism. It is worth noting that the heat generated by the phase change will be taken into account in the internal energy term of Eq. (B1) and not as a volumetric heat source. Thus the heat input term becomes:

$$\dot{Q} = -\int_{C.S.} (-k\nabla T)\cdot\breve{n} \, dA \tag{B5}$$

From Eqs. (B1), (B4) and (B5), and grouping the control surface flow terms we obtain:

$$\int_{C.S.} \frac{d}{dt}\left[\rho\left(c_p T - p/\rho\right)\right] dV = -\int_{C.S.} \frac{d}{dt}\left(\rho c_p T\vec{v} - k\nabla T\right)\cdot\breve{n} \, dA \tag{B6}$$

The reaction enthalpy generated during the sorption process involving a mass of hydrogen S_m is expressed by:

$$S_m c_{ps} T - S_m c_{pg} T = S_m \Delta H(T) \approx S_m \Delta H\left(T_{ref}\right) \tag{B7}$$

where c_{pg} and c_{ps} are the gas and solid phase heat capacity at constant pressure respectively, and $\Delta H(T_{ref})$ is the reaction enthalpy at reference temperature, which is considered constant in the operational temperature range.

The container is a multiphase system that can undergo phase changes. At first glance we have a solid phase and a gaseous phase. Strictly speaking there is more than one solid phase as the solid material can be heat conductive material (e.g.: aluminum foam), hydride and hydride forming alloy. At this point we shall not consider heat conductive material, it will be added later as a modification to avoid unnecessary complications.

Here we will consider the hydride forming alloy and the hydride as a single solid material. We will also consider that the porosity ε of this solid material remains constant, i.e. the density of the solid ρ_s varies only though hydrogen mass gains or losses in order to achieve conservation of mass. This is an important simplification as the alloy usually undergoes a significant volume increase during the hydriding (See section A.3).

If we model the system as a two-phase mixture [57] Eq. (B6) then becomes:

$$\int_{C.V.} \frac{d}{dt}\left[\varepsilon\left(\rho_g c_{pg} T - \frac{P}{\rho}\right) + (1-\varepsilon)\left(\rho_s c_{ps} T\right)\right] dV = -\int_{C.S.} \left(\rho_g c_{pg} T\vec{v} - k_{eff}\nabla T\right)\cdot\breve{n} \, dA \tag{B8}$$

We shall disregard the variation of total internal energy due to variation of the gas density ($\varepsilon c_{pg} T d\rho_g/dt$) as the total internal energy of the gas phase is relatively unimportant. We therefore obtain:

$$\int_{C.V.} \left[\varepsilon\left(\rho_g c_{pg}\frac{dT}{dt} - \frac{1}{\rho}\frac{dP}{dt}\right) + (1-\varepsilon)\left(\rho_s c_{ps}\frac{dT}{dt}\right) + (1-\varepsilon)\left(\frac{d\rho_s}{dt}c_{ps}T\right)\right] \times dV = -\int_{C.S.} \left(\rho_g c_{pg} T\vec{v} - k_{eff}\nabla T\right)\cdot\breve{n} \, dA \tag{B9}$$

In the sorption process, gas is added or extracted from the solid phase. As we have taken a constant value of ε and given that no solid mass crosses the control volume boundaries, the sorption process has to occur through a variation of the solid density ρ_s. Therefore the mass of gas per unit volume and per unit time involved in the sorption process S_m has to satisfy:

$$S_m = -(1-\varepsilon)\frac{d\rho_s}{dt} \tag{B10}$$

From Eqs. (B7), (B9) and (B10) we obtain:

$$\int_{C.V.} \left[\varepsilon\left(\rho_g c_{pg}\frac{dT}{dt} - \frac{1}{\rho}\frac{dp}{dt}\right) + (1-\varepsilon)\left(\rho_s c_{ps}\frac{dT}{dt}\right)\right] dV = \int_{C.V.} \left(S_m \Delta H + S_m c_{pg} T\right) dV - \int_{C.S.} \left(\rho_g c_{pg} T\vec{v} - k_{eff}\nabla T\right)\cdot\breve{n} \, dA \tag{B11}$$

We are interested in developing a one-dimensional model as represented in Figure B1, where heat transfer occurs in the main dimension and convective effects can be disregarded. We consider all properties to vary only in the main dimension while being uniform in the others. The changes of ρ_g and ε will be neglected and we will assume there are no convective flows in the direction of the main dimension, then the continuity equation for the gas phase reduces to:

$$\int_{C.V.} S_m \, dV = \int_{C.S.} \rho_g \vec{v}\cdot\breve{n} \, dA \tag{B12}$$

In our one-dimensional model we consider temperature and heat capacity to be homogeneous in the control volume, obtaining:

$$\int_{C.V.} S_m c_{pg} T \, dV = \int_{C.S.} \rho_g c_{pg} T\vec{v}\cdot\breve{n} \, dA \tag{B13}$$

This equation states that the net sensible heat of the gas crossing the control surface is the same sensible heat of the gas that participates in the sorption reaction. This is true here because we are not considering changes in gas density, or gas flows, in the main dimension x.

For a one-dimensional system in x with transversal area A and thickness dx, and using the relation of Eq. (B13), Eq. (B11) becomes:

$$\left[\varepsilon\left(\rho_g c_{pg}\frac{dT}{dt}-\frac{1}{\rho}\frac{dP}{dt}\right)+(1-\varepsilon)\left(\rho_s c_{ps}\frac{dT}{dt}\right)\right]A\,dx = S_m\,\Delta H\,A\,dx-\left(k_{eff}\nabla T\right)_{x+dx}A+\left(k_{eff}\nabla T\right)_x A \quad (B14)$$

Finally, we rewrite Eq. (B14) to get the one-dimensional heat equation for a finite volume $dV = Adx$:

$$\left(\varepsilon\rho_g c_{pg}+(1-\varepsilon)\rho_s c_{ps}\right)\frac{dT}{dt}=\frac{\varepsilon}{\rho}\frac{dP}{dt}+S_m\Delta H+\frac{\left(k_{eff}A\nabla T\right)_x-\left(k_{eff}A\nabla T\right)_{x+dx}}{dV} \quad (B15)$$

If we now introduce a non-porous conductive material d in a volumetric fraction F, the effective properties of the mixture will be modified. We will hopefully see an increase of the thermal conductivity in the direction of the main dimension, a variation of the heat capacity, and a small reduction of the overall hydrogen storing capacity. In a previous work we explored the compromise between the increase of thermal conductivity and the reduction of storage capacity, proposing a method to define the optimum amount of conductive material [30].

The effective thermal conductivity k_{eff} now depends on the thermal conductivity of the gas–solid mixture, but more significantly on the thermal conductivity of the added conductive material and its geometry. If the material is placed forming a continuous thermal path in the direction of the heat flow (maximum effective conductivity) we can write:

$$k_{eff}=(\varepsilon k_g+(1-\varepsilon)k_s)(1-F)+k_d F \quad (B16)$$

Notice here that we have also assumed a continuous thermal path for the solid (hydride) which normally is a powder, yet its contribution to the total thermal conductivity is low and this does not bring a relevant error. Additionally we consider that the distance between hydride and conductive material is small enough to be irrelevant.

The effective heat capacity $(\rho c_p)_{eff}$ of the new mixture will be:

$$\left(\rho c_p\right)_{eff}=\left(\varepsilon\rho_g c_{pg}+(1-\varepsilon)\rho_s c_{ps}\right)(1-F)+\rho_d c_{pd}F, \quad (B17)$$

and the reacting mass of hydrogen rate per unit volume of the mixture now becomes:

$$S_m=(1-\varepsilon)(1-F)C_{sg}\rho_s\frac{dX}{dt} \quad (B18)$$

Finally we get the equation including the conductive material, i.e. the one-dimensional thermal equation that will be used in our model.

$$\left(\rho c_p\right)_{eff}\frac{dT}{dt}=\frac{\varepsilon(1-F)}{\rho}\frac{dP}{dt}+S_m\Delta H+\frac{\left(k_{eff}A\nabla T\right)_x-\left(k_{eff}A\nabla T\right)_{x+dx}}{dV} \quad (B19)$$

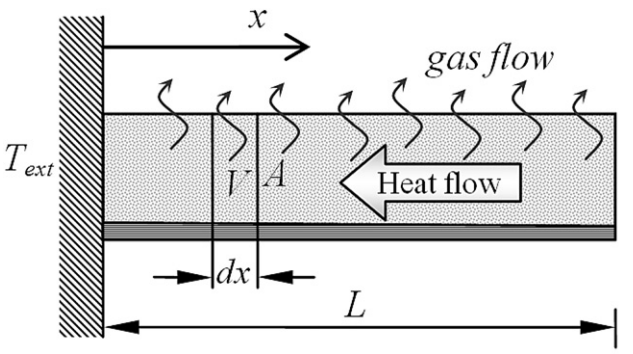

Figure B1 – One-dimensional model.

Appendix C. Reference information

The parameters from references used for simulations of Section 3.4 are depicted in Table C1. There is also a brief discussion of the assumptions made in each case.

- Visaria-a [50]

This study assumes a linear increase of pressure during the first minute of the absorption reaction; we considered constant absorption pressure.

As we did not consider convection coefficient nor thermal contact resistance, the condition more comparable of this reference is $h_f = 5000\ W\ m^{-2}\ K^{-1}$ and $R_{tc} = 0$.

We considered k_{eff} according to Eq. (2) of this paper: $k_{eff} = 0.51\ W\ m^{-1}\ K^{-1}$

- Visaria-b [47]

From the text we know that the maximum distance from the heat exchange surfaces and the hydride is $L \approx 15$ mm.

From Fig. 6 of this reference we obtain $P_e = 160$ bar and $T_{max} = 51\ ^\circ C$.

According to Test 2 of the reference, $T_{ext} \approx 20\ ^\circ C$.

We considered constant absorption pressure.

Reaction time is about 20 min according to the text and to Fig. 12 of the reference.

We considered $k_{eff} = 0.51\ W\ m^{-1}\ K^{-1}$.

- Melnichuk [30,58]

$t_{90\%} = 3.5$ min according to Fig. 9 of the reference
$L_{cont} = 3 \times 10^{-2}$ m
$F_{cont} = 0.33$
$k_{eff} = 10\ W\ m^{-1}\ K^{-1}$ (calculated with Eq. (B16)).

- Melnichuk# [30,58]

$L_{pore} = 3.25 \times 10^{-3}$ m

$F_{pore} = 0$
$k_{eff} = 0.15\ W\ m^{-1}\ K^{-1}$.

- Laurencelle [55]

$t_{90\%} = 1.7$ min according to Fig. 7 of the reference
$L_{cont} = 6.35 \times 10^{-3}$ m
$F_{cont} = 0.09$
$k_{eff} = 16.16\ W\ m^{-1}\ K^{-1}$.

- Laurencelle# [55]

$L_{pore} = 1.15 \times 10^{-3}$ m (aluminum foam 40 ppi)
$F_{pore} = 0$
$k_{eff} = 0.15\ W\ m^{-1}\ K^{-1}$.

- Verga [34]

$L \approx 6$ mm from Fig. 5 (a further improvement of the method used to estimate L for a complex geometry is out of the scope of this paper)
$k_{eff} = 0.4\ W\ m^{-1}\ K^{-1}$
$t_{90\%} = 7.5$ min from Fig. 1 and the text of the reference.

- Capurso [35]

$L = 3.5 \times 10^{-3}$ m considering that heat is only removed from the lateral walls of the experimental device of the reference.
$T_{ext} \approx 270$ °C without considering thermal resistance of contact between pellets and experimental device.

- Chaise [33]

$k_{eff} = 1\ W\ m^{-1}\ K^{-1}$ from Fig. 6 of the reference for the case "C" (using 5 wt% ENG)
$t_{90\%} = 20$ min according to Fig. 13 of the reference
T_{ext} is assumed 20 °C (air at room temperature used as coolant).

REFERENCES

[1] Winter CJ. After nuclear has gone – energy in Germany. Int J Hydrogen Energy 2012;37:1–5.
[2] Heung L. "Using metal hydride to store hydrogen". Web site: http://sti.srs.gov/fulltext/ms2003172/ms2003172.pdf.
[3] Mazumdar S, Ram Gopal M, Bhattacharyya S. Thermodynamic analysis and optimization of compressor-driven metal hydride cooling systems. Int J Hydrogen Energy 2005;30:631–41.
[4] Gondor G, Lexcellent C. Analysis of hydrogen storage in metal hydride tanks introducing an induced phase transformation. Int J Hydrogen Energy 2009;34:5716–25.
[5] Kikkinides ES, Georgiadis MC, Stubos AK. On the optimization of hydrogen storage in metal hydride beds. Int J Hydrogen Energy 2006;31:737–51.
[6] Freni A, Cipitì F, Cacciola G. Finite element-based simulation of a metal hydride-based hydrogen storage tank. Int J Hydrogen Energy 2009;34:8574–82.
[7] Krokos CA, Nokolic D, Kikkinides ES, Georgiadis MC, Stubos AK. Modeling and optimization of multi-tubular metal hydride beds for efficient hydrogen storage. Int J Hydrogen Energy 2009;43:9128–40.
[8] Servaraj NB, Chapelle D, Perreux D, Figiel H. Modelling the evolution of temperature inside $LaNi_{4.78}Sn_{0.22}$ storage tank during refueling. Mater Des 2009;30:954–7.
[9] Yang FS, Zhang ZX, Wang GX, Bao ZW, Diniz da Costa JC, Rudolph V. Numerical study of a metal hydride heat transformer for low-grade heat recovery simulation of a MH heat transformer. Appl Therm Eng 2011;31(14–15):2749–56.
[10] Muthukumar P, Prakash Maiya M, Srinivasa Murthy S. Experiments on a metal hydride-based hydrogen storage device. Int J Hydrogen Energy 2005;30:1569–81.
[11] Kim KJ, Montoya B, Razani A, Lee K-H. Metal hydride compacts of improved thermal conductivity. Int J Hydrogen Energy 2001;26:609–13.
[12] Chen Y, Sequeira CA, Chen C, Wang X, Wang Q. Metal hydride beds and hydrogen supply tanks as minitype PEMFC hydrogen sources. Int J Hydrogen Energy 2003;28:329–33.
[13] Mohan G, Prakash Maiya M, Srinivasa Murthy S. Performance simulation of metal hydride hydrogen storage device with

Table C1 – Parameters from reference.

Parameters	$Ti_{1.1}CrMn$		$LaNi_5$				Mg		
Given name	Visaria-a	Visaria-b	Melnichuk	Melnichuk#	Laurencelle	Laurencelle#	Verga	Capurso	Chaise
$t_{90\%}$ (s)	750	1200	210	210	102	102	450	850	1200
P_g (bar)	300	280	30	30	12.73	12.73	6	8	10
P_e (bar)	162	160	5.2	5.2	5.2	5.2	0.8	0.57	1.4
T_{max} (°C)	55	51	109	109	78	78	359	372	382
T_{ext} (°C)	20	20	50	50	50	50	280	270	320
L (m)	0.015	0.015	0.00325	0.03	0.00115	0.00635	0.006	0.0035	0.005
k_{eff} (W m^{-1} K^{-1})	0.51	0.51	0.15	10	0.15	16.16	0.3	0.35	1
c_{ps} (J kg^{-1}K^{-1})	500	500	355	355	355	355	120	120	120
ΔH^n (J mol^{-1})	−14,390	−14,390	−30,478	−30,478	−30,478	−30,478	−75,000	−75,000	−75,000
ΔS (J mol^{-1} K^{-1})	−91.3	−91.3	−108	−108	−108	−108	−133.5	−133.5	−133.5
C_{sg}	0.015	0.015	0.0128	0.0128	0.0128	0.0128	0.06	0.06	0.06
ρ_s (kg m^{-3})	6200	6200	8310	8310	8310	8310	1740	1740	1740
ε	0.6	0.6	0.55	0.55	0.55	0.55	0.7	0.5	0.5
F	0	0	0.33	0	0.09	0	0	0.05	0.05
E_{Abs} (J mol^{-1})	20,700	20,700	21,170	21,170	21,170	21,170	1.24×10^5	1.24×10^5	1.24×10^5
κ_{Abs} (s^{-1})	150	150	59.2	59.2	59.2	59.2	2.90×10^8	2.90×10^8	2.90×10^8
Reference	[50]	[47,50]	[30,56]	[30]	[52]	[52]	[34,37]	[35,37]	[33,37]

embedded filters and heat exchanger tubes. Int J Hydrogen Energy 2007;32:4978–87.
[14] Laurencelle F, Dehouche Z, Morin F, Goyette J. Experimental study on a metal hydride based hydrogen compressor. J Alloys Compd 2009;475:810–6.
[15] Dhaou H, Souahlia A, Mellouli S, Askri F, Jemni A, Ben Nasrallah S. Experimental study of a metal hydride vessel based on a finned spiral heat exchanger. Int J Hydrogen Energy 2010;35:1674–80.
[16] Muthukumar P, Madhavakrishna U, Dewan A. Parametric studies on a metal hydride based hydrogen storage device. Int J Hydrogen Energy 2007;32:4988–97.
[17] Mat MD, Kaplan Y. Numerical study of hydrogen absorption in an Lm–Ni_5 hydride reactor. Int J Hydrogen Energy 2001;26:957–63.
[18] Aldas K, Mat D, Kaplan Y. A three-dimensional mathematical model for absorption in a metal hydride bed. Int J Hydrogen Energy 2002;27:1049–56.
[19] Asakuma Y, Miyauchi S, Yamamoto T, Aoki H, Miura T. Homogenization method for elective thermal conductivity of metal hydride bed. Int J Hydrogen Energy 2004;29:209–16.
[20] Askri F, Jemni A, Ben Nasrallah S. Dynamic behavior of metal–hydrogen reactor during hydriding process. Int J Hydrogen Energy 2004;29:635–47.
[21] Askri F, Jemni A, Ben Nasrallah S. Prediction of transient heat and mass transfer in a closed metal–hydrogen reactor. Int J Hydrogen Energy 2004;29:195–208.
[22] Demircan A, Demiralp M, Kaplan Y, Mat MD, Veziroglu TN. Experimental and theoretical analysis of hydrogen absorption in $LaNi_5$–H_2 reactors. Int J Hydrogen Energy 2005;30:1437–46.
[23] Botzung M, Chaudourne S, Gillia O, Perret C, Latroche M, Percheron-Guegan A, et al. Simulation and experimental validation of a hydrogen storage tank with metal hydrides. Int J Hydrogen Energy 2008;33:98–104.
[24] Brown TM, Brouwer J, Samuelsen GS, Holcomb FH, King Joel. Accurate simplified dynamic model of a metal hydride tank. Int J Hydrogen Energy 2008;33:5596–605.
[25] Gambini M, Manno M, Vellini M. Numerical analysis and performance assessment of metal hydride-based hydrogen storage systems. Int J Hydrogen Energy 2008;33:6178–87.
[26] Chung CA, Hoa Ci-Jyun. Thermal–fluid behavior of the hydriding and dehydriding processes in a metal hydride hydrogen storage canister. Int J Hydrogen Energy 2009;34:4351–64.
[27] Førde T, Næss E, Yartys VA. Modelling and experimental results of heat transfer in a metal hydride store during hydrogen charge and discharge. Int J Hydrogen Energy 2009;34:5121–30.
[28] Mellouli S, Askri F, Dhaou H, Jemni A, Ben Nasrallah S. Numerical simulation of heat and mass transfer in metal hydride hydrogen storage tanks for fuel cell vehicles. Int J Hydrogen Energy 2010;35:1693–705.
[29] Melnichuk M, Silin N, Andreasen G, Corso HL, Visintin A, Peretti HA. Hydrogen discharge simulation and testing of a metal-hydride container. Int J Hydrogen Energy 2010;35:5855–9.
[30] Melnichuk M, Silin N, Peretti HA. Optimized heat transfer fin design for a metal-hydride hydrogen storage container. Int J Hydrogen Energy 2009;34:3417–24.
[31] Tsai M-L, Yang T-S. On the selection of metal foam volume fraction for hydriding time minimization of metal hydride reactors. Int J Hydrogen Energy 2010;35:11052–63.
[32] Wang Y, Adroher XC, Chen J, Yang XG, Miller T. Three-dimensional modeling of hydrogen sorption in metal hydride hydrogen storage beds. J Power Sources 2009;194:997–1006.
[33] Chaise A, de Rango P, Marty P, Fruchart D, Miraglia S, Olivès R, et al. Enhancement of hydrogen sorption in magnesium hydride using expanded natural graphite. Int J Hydrogen Energy 2009;34:8589–96.
[34] Verga M, Armanasco F, Guardamagna C, Valli C, Bianchin A, Agresti F, et al. Scaling up effects of Mg hydride in a temperature and pressure-controlled hydrogen storage device. Int J Hydrogen Energy 2009;34:4602–10.
[35] Capurso G, Agresti F, Lo Russo S, Maddalena A, Principi G, Cavallari A, et al. Performance tests of a small hydrogen reactor based on Mg–Al pellets. J Alloys Compd 2011;509(2):646–9.
[36] Garrier S, Chaise A, de Rango P, Marty P, Delhomme B, Fruchart D, et al. MgH_2 intermediate scale tank tests under various experimental conditions. Int J Hydrogen Energy 2011;36:9719–26.
[37] Marty P, Fourmigue J-F, De Rango P, Fruchart D, Charbonnier J. Numerical simulation of heat and mass transfer during the absorption of hydrogen in a magnesium hydride. Energy Convers Manage 2006;47:3632–43.
[38] Lozano GA, Eigen N, Keller C, Dornheim M, Bormann R. Effects of heat transfer on the sorption kinetics of complex hydride reacting systems. Int J Hydrogen Energy 2009;34:1896–903.
[39] Ahluwalia RK, Hua TQ, Peng JK. On-board and Off-board performance of hydrogen storage options for light-duty vehicles. Int J Hydrogen Energy 2012;37:2891–910.
[40] Mosher DA, Arsenault S, Tanga X, Anton DL. Design, fabrication and testing of $NaAlH_4$ based hydrogen storage systems. J Alloys Compd 2007;446–447:707–12.
[41] Leela Mohana Reddy A, Ramaprabhu S. Design and fabrication of carbon nanotube-based microfuel cell and fuel cell stack coupled with hydrogen storage device. Int J Hydrogen Energy 2007;32:4272–8.
[42] Ye J, Jiang L, Li Z, Liu X, Wang S, Li X. Numerical analysis of heat and mass transfer during absorption of hydrogen in metal hydride based hydrogen storage tanks. Int J Hydrogen Energy 2010;35:8216–24.
[43] Park J-G, Jang K-J, Lee PS, Lee J-Y. The operating characteristics of the compressor-driven metal hydride heat pump system. Int J Hydrogen Energy 2001;26:701–6.
[44] Chernov IA, Gabis IE. Mathematical model of metal-hydride hydrogen tank with quick sorption. J Alloys Compd 2011;509:809–11.
[45] Visaria M, Mudawar I. Coiled-tube heat exchanger for high-pressure metal hydride hydrogen storage systems – part 1. Experimental study. Int J Heat Mass Transf 2012;55:1782–95.
[46] Fateev GA, Jang K-J, Park J-G, Han S-C, Lee Paul, Lee J-Y. Techniques for metal hydride thermal energy conversion and their optimization. J Alloys Compd 2000;313:174–81.
[47] Oi T, Maki K, Sakaki Y. Heat transfer characteristics of the metal hydride vessel based on the plate-fin type heat exchanger. J Power Sources 2004;125:52–61.
[48] Mayer U, Groll M, Supper W. Heat and mass transfer in metal hydride reaction beds: experimental and theoretical results. J Less-Common Met 1987;131:235–44.
[49] Chaise A, Marty P, de Rango P, Fruchart D. A simple criterion for estimating the effect of pressure gradients during hydrogen absorption in a hydride reactor. Int J Heat Mass Transf 2009;52:4564–72.
[50] Visaria M, Mudawar I, Pourpoint T, Kumar S. Study of heat transfer and kinetics parameters influencing the design of heat exchangers for hydrogen storage in high-pressure metal hydrides. Int J Heat Mass Transf 2010;53:2229–39.
[51] Satyapal S, Petrovic J, Read C, Thomas G, Ordaz G. The U.S. Department of Energy's National hydrogen storage Project: progress towards meeting hydrogen-powered vehicle requirements. Catal Today 2007;120:246–56.
[52] Larson RE, Higdon JJL. Microscopic flow near the surface of two-dimensional porous media. Part l. Axial flow. J Fluid Mech 1986;166:444–72.

[53] Cannon JR. The one dimensional heat equation. Addison-Wesley Publishing Company; 1984. p. 281.
[54] Askri F, Jemni A, Ben Nasrallah S. Study of two-dimensional and dynamic heat and mass transfer in a metal–hydrogen reactor. Int J Hydrogen Energy 2003;28:337–57.
[55] Laurencelle F, Goyette J. Simulation of heat transfer in a metal hydride reactor with aluminium foam. Int J Hydrogen Energy 2007;32:2957–64.
[56] Cengel YA, Boles MA. Termodinámica. 5th ed. McGraw Hill; 2006. p. 256.
[57] Ishii M, Hibiki T. Thermo-fluid dynamics of two-phase flow. 1st ed. Springer; 2006. p. 384.
[58] Melnichuk M. "Estudio numérico y experimental de almacenadores de hidrógeno basados en hidruros metálicos". Thesis work, Balseiro Institute, CENA-Univ. Nac. de Cuyo, 2010. pp. 79–89. Available on-line at: http://ricabib.cab.cnea.gov.ar/132/.
[59] Züttel A, Borgschulte A, Schlapbach L. Hydrogen as a future energy carrier. WILEY-VCH Verlag GmbH & Co. KGaA; 2008. p. 81.